Rotation Symmetry Group Detection
Via Frequency Analysis of Frieze-Expansions

Seungkyu Lee†
sklee@psu.edu

Robert T. Collins†
rcollins@cse.psu.edu

Yanxi Liu*†
yanxi@cse.psu.edu

†Dept. of Computer Science and Engineering *Dept. of Electrical Engineering
The Pennsylvania State University

Abstract

We present a novel and effective algorithm for rotation symmetry group detection from real-world images. We propose a frieze-expansion method that transforms rotation symmetry group detection into a simple translation symmetry detection problem. We define and construct a dense symmetry strength map from a given image, and search for potential rotational symmetry centers automatically. Frequency analysis, using Discrete Fourier Transform (DFT), is applied to the frieze-expansion patterns to uncover the types and the cardinality of multiple rotation symmetry groups in an image, concentric or otherwise. Furthermore, our detection algorithm can discriminate discrete versus continuous and cyclic versus dihedral symmetry groups, and identify the corresponding supporting regions in the image. Experimental results on over 80 synthetic and natural images demonstrate superior performance of our rotation detection algorithm in accuracy and in speed over the state of the art rotation detection algorithms.

1. Introduction

Symmetry is ubiquitous in natural and man-made images. Symmetric figures attract human attention within natural scenes [16]. Automatic symmetry detection on 2D or 3D images has been an active research area for over four decades [1, 2, 3, 4, 5, 11]. Symmetry is a type of shape
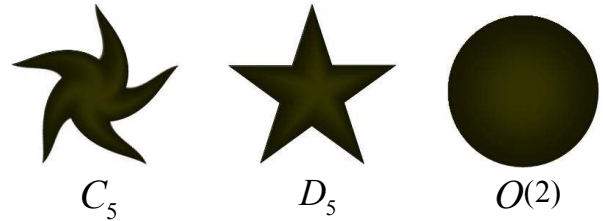

Figure 1: Different rotation symmetry groups. C_n: n-fold cyclic group (pure rotation symmetry). D_n: n-fold dihedral group (rotation + reflection symmetry) that contains a cyclic group (C_n). $O(2)$: Continuous rotation with infinite reflection symmetries.

regularity that plays an important role for object recognition and classification in computer vision [17]. A symmetric object can be characterized efficiently by its symmetry groups, yielding a low dimensional set of features for object representation, recognition, matching, segmentation and tracking.

Figure 1 shows examples of the three distinct types of rotation symmetry groups about a fixed point in 2D Euclidean space [14]. We present a novel approach for detecting the three types of rotation symmetry groups in real world images. Our work makes the following specific contributions: (1) we propose a novel frieze-expansion method (Figure 2), which converts 2D rotational symmetry detection into a problem of 1D translation symmetry detection; (2) We propose a rotation symmetry strength (RSS) function that can be used to recursively evaluate potential centers of rotation symmetry on any given image; (3) our algorithm detects and discriminates all three rotation
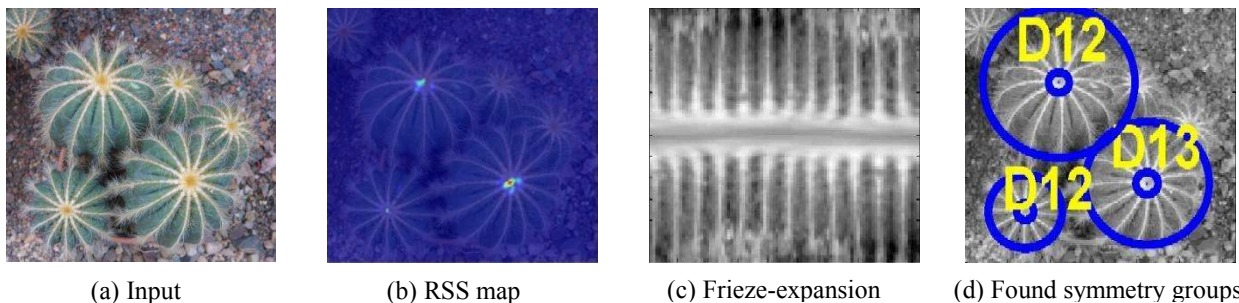

Figure 2: (a) Test image with multiple rotational centers and symmetry types. (b) Rotation Symmetry Strength (RSS) map overlaid on the original image (c) One sample of Frieze-expansion (d) Rotation symmetry group detection result

symmetry groups using frequency domain analysis on the frieze-expansion patterns. Figure 2 demonstrates a sample rotation symmetry detection process from a natural photo. We evaluate our algorithm on more than 80 synthetic/real world images with single/multiple rotation centers and compare against the state of the art rotation detection algorithms (Section 5).

2. Previous Work

Symmetry detection and analysis has been a research topic not only in computer vision but also in mathematics, architecture, art and sciences [10]. In computer vision, many rotation symmetry detection algorithms have been proposed for 2D and 3D images [1, 2, 3, 4, 5, 11].

Some recent work [1, 2, 3] proposes to use local features such as edge, corner and boundary information for symmetry detection. In [3] the authors use local features from Gradient Vector Flow (GVF) to build a confidence map to detect rotation symmetry centers. Loy and Eklundh [1] use SIFT features to determine rotation symmetry centers. These local feature-based algorithms can be fast, however, selected local features are not always optimal for symmetry detection. For example, Loy and Eklundh [1], using SIFT features as key points, would fail to capture symmetric objects consisting of textureless regions (images I-5, I-6 and I-7 in Figure 9). They also frequently yield false positive incorrect symmetry centers supported only by very few points (2 or 3).

Other approaches [4, 5, 11] search either the entire image or the whole parameter space. For example, the symmetry detection algorithm introduced for digital Papercutting [4] uses an edge-based feature set and searches through the whole 2D polar parameter space of reflection axes. These

algorithms usually take much longer than local feature based algorithms, which is perhaps their biggest drawback. Autocorrelation has been used for symmetry detection for several applications [4, 7, 11]. Autocorrelation is useful for periodic pattern detection and has been used for signal processing [13]. Liu et al [7] introduce *region of dominance* to detect translation symmetry of frieze and wallpaper patterns, where autocorrelation is computed in frequency domain based on the Wiener-Khinchin [13] theorem.

As a frequency-based symmetry detection algorithm, Keller and Shkolnisky [5]'s work is the most similar to ours. They use a polar fast Fourier transform (FFT) on the pseudo-polar grid to find signal repetition over angular direction for rotation symmetry detection. However, their polar FFT investigates pre-selected local areas and can not detect all existing symmetry types at different locations. They can not distinguish cyclic from dihedral symmetry, and are limited to detecting a single symmetry in each image.

Table 1 shows a categorized comparison of our proposed algorithm with several state of the art rotation symmetry detection algorithms.

3. Rotation Symmetry Detection

In our work, a rotation symmetry group is characterized by the following four properties.
1) Center of rotation symmetry,
2) Number of fold (cardinality of the symmetry group),
3) Type of symmetry group (Dihedral/Cyclic/O(2)), and
4) Local supporting region (annulus).

Our algorithm detects these four properties in two steps: rotation center detection and symmetry group analysis. A rotation symmetry-strength (RSS) map represents the symmetry strength at each pixel of the image by a 2D weighted map. Rotation center detection finds peaks in the RSS map. From the detected centers of rotation, a symmetry analysis step detects the rest of the symmetry group properties.

3.1. Frieze-Expansion

The existence of a rotational symmetry is usually supported by an annulus with or without a connected center point. If there is rotation symmetry about the center, this annulus contains repeating patterns along its circular direction (Figure 3 (a),(b)). In this work, we propose to detect rotation symmetry in a transformed space of the original image via frieze-expansion where the rotation symmetry on the circular band becomes translation symmetries on a frieze-expansion pattern (Figure 3 (b)). Given the location of a candidate rotation center, a diameter and a polar angle-step size (Figure 3 (a)), we re-align each diameter in parallel, from left to right, to form a horizontal pattern while advancing about the center angularly in the

Detection	GVF [3]	Papercut [4]	SIFT [1]	FFT [5]	Ours
Dihedral /Cyclic/O(2)?	No	*	No	No	**Yes**
Concentric symmetry?	No	**Yes**	No	No	**Yes**
Symmetry map?	**Yes**	**Yes**	No	No	**Yes**
Time complexity **	$O(B^{K-1}+I)$	O(K+I)	O(P+I)	O(I)	O(I)
Processing time (sec.) ***	150	50	3	****	25

Table 1: Comparison of the state of the art rotation symmetry detection algorithms *[4] is designed to detect dihedral and frieze groups only. **I(image size), P(number of key points), K(number of folds). B(see [3]) *** the average computing time on ten 150x150 images with a single rotation symmetry center. ****Information unavailable
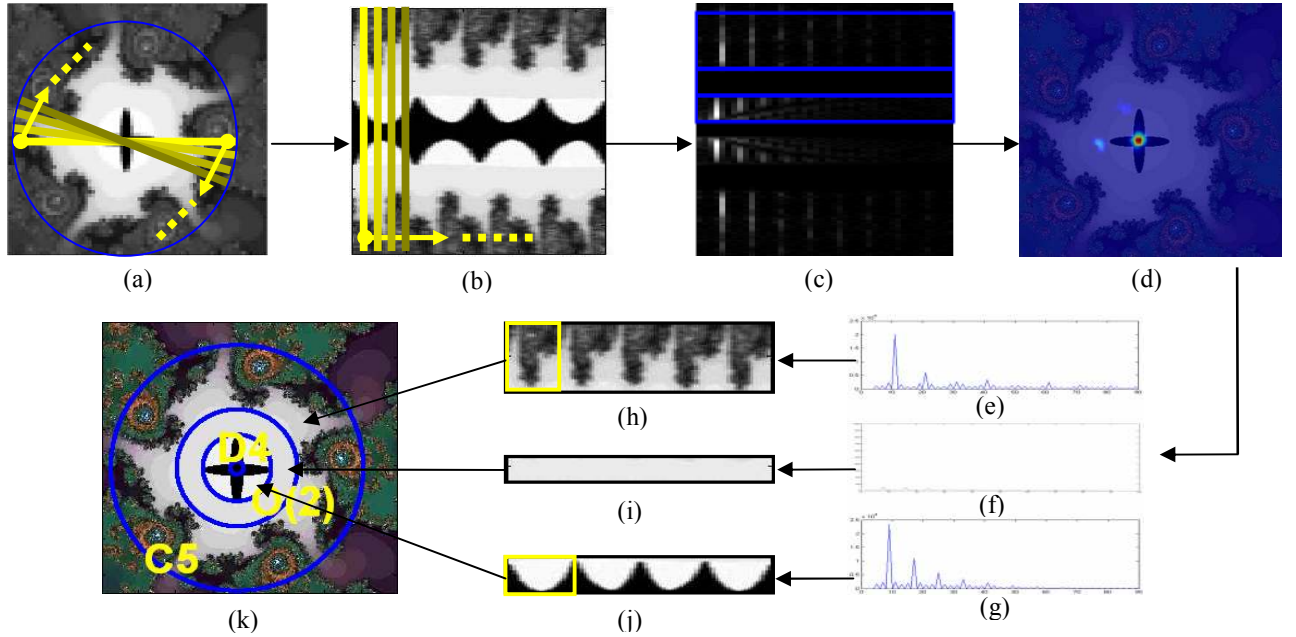
Figure 3: (a) Original image; a region is selected with the correct symmetry center. (b) Frieze-expansion; each diameter of the circle corresponds to a column of the frieze-expansion. (c) 1D DFT results; horizontal axis is the index of DFT basis and vertical axis is the same as the vertical axis of the frieze pattern. (a)~(c) are repeated for all image pixels to build RSS map. (d) Rotation symmetry strength (RSS) map overlaid on the original image. Once a center is detected, the corresponding DFT segmentation is performed on (c). (e)(f)(g) are the sum of absolute DFT coefficients of the segmented regions. (h)(i)(j) are the segmented frieze patterns from (b). (k) Final rotation symmetry group detection result.

original image (Figure 3(b)). If the candidate center location in the original image is indeed the center of a rotational symmetry, the converted frieze-expansion image becomes a true frieze pattern with non-trivial horizontal translation symmetry, and vice versa.

Dihedral and cyclic groups are the only discrete rotation symmetry groups and O(2) is the only continuous symmetry group in 2D. There is a unique relation between the discrete rotation symmetry groups and frieze patterns. Frieze patterns have seven distinct symmetry groups [9]. If there is a rotation symmetry in an image, its frieze-expansion should fall into one of these seven groups. In other words, all types of frieze patterns, if we convert them back into circular
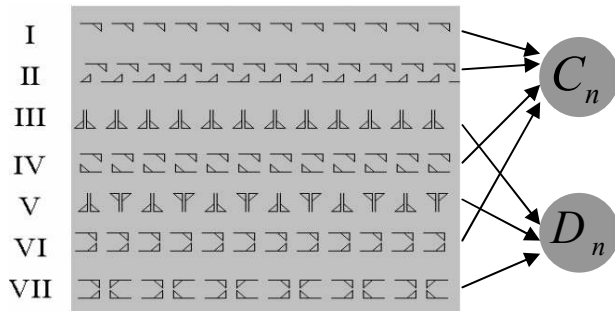

Figure 4: The correspondence between the seven frieze groups and the two rotation symmetry groups in 2D.

regions, must have some type of rotation symmetry. This relation is used for our rotation symmetry analysis. Figure 4 shows the seven frieze groups and their corresponding rotational symmetry groups.

3.2. Discrete Fourier Transform

We are now facing the task of translation symmetry detection or frequency detection from a special type of patterns: frieze-expansions. Two predominant approaches for translation symmetry analysis, among many other alternatives, are the discrete Fourier transform (DFT) method in the frequency domain and the auto-correlation method in the spatial domain. Based on Wiener-Khinchin theorem [13], we can establish the equivalence relation between the spectral density and the DFT of AC for the same input signal as follows (Figure 5):

We perform a one-dimensional horizontal discrete Fourier transform (DFT) on each row of the frieze-expansion. The DFT coefficients are defined in Equations (1) and (2) below [12]:

$$X(k) = a(k) + ib(k) = \sum_{n=0}^{N-1} x(n)e^{-i\frac{2\pi}{N}n(k-1)} \qquad (1)$$

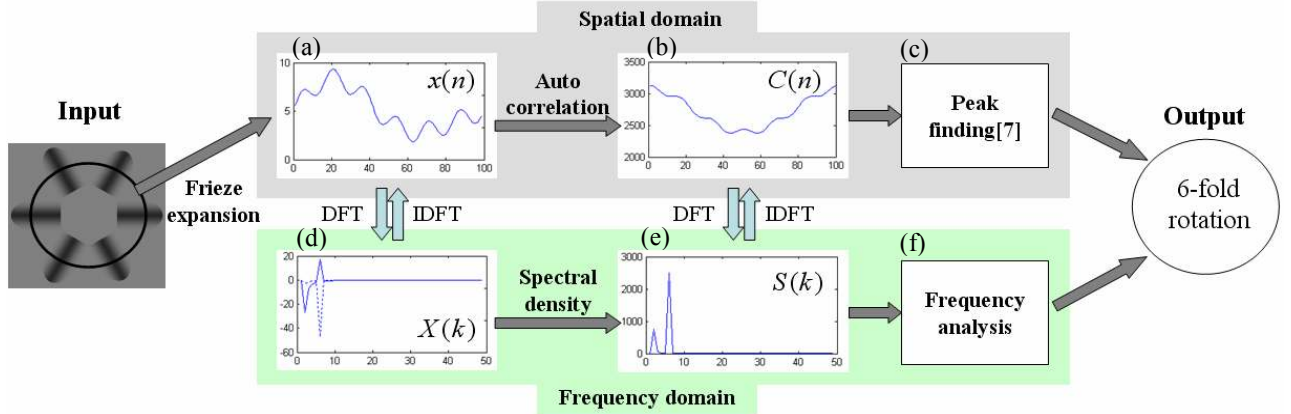$$S(k) = \overline{X(k)}X(k) = a(k)^2 + b(k)^2 \qquad (2)$$

Figure 5: Relation between spectral density S(k) and autocorrelation C(n). ((a)->(d)->(e)->(f)) is the processes of our algorithm, which is equivalent to using the DFT of autocorrelation ((a)->(b)->(e)->(f)). Peak finding algorithms [7] use (a)->(d)->(e)->(b)->(c) to reduce the time complexity. *DC coefficients are not shown.*

where X(k) is k[th] coefficient of DFT (a(k) is real part and b(k) is imaginary part of the coefficient), N is the width of the frieze-expansion pattern and x(n) is the intensity value along a single row of the frieze-expansion. S(k) is the energy spectral density of the kth DFT component.

X(k) corresponds to the relative strength of all corresponding potential frequency. If one specific coefficient has a dominant peak value, there exists a translational symmetry in that x(n) row of the frieze-expansion. All possible phase differences between x(n) and one of the corresponding DFT components (sine or cosine wave) are inbetween 0 and $\pi/2$, which can be calculated by its spectral density from both sine and cosine waves of the same frequency. Due to the symmetric nature of DFT coefficients, only the first half of the set of the coefficients needs to be checked.

The relation between the spectral density S(k) and the auto-correlation C(n) can thus be expressed as (also shown graphically in Figure 5):

$$C(n) = \sum_{m=0}^{N-1} \overline{x(m)} x(n+m) = \sum_{k=0}^{N-1} S(k) e^{i\frac{2\pi}{N}k(n-1)} \quad (3)$$

From (3) one can verify that autocorrelation and spectral density represent the same information in different domains. DFT decomposes autocorrelation into a set of frequency components with the highest coefficient assigned to the strongest component. Previous work [7] has used auto-correlation for finding the underlying lattice (translation symmetry) in frieze and wallpaper patterns via inverse FFT of the spectral density (for computational efficiency).

Frequency analysis on the spectral density investigates regularity of autocorrelation by correlating with densely defined components (sine and cosine waves) rather than detecting coarse peak locations. Strong response to a DFT component means that there is a set of peaks or regular variation of corresponding frequency in the spatial domain. We do not have to compare all pairs of local maximum autocorrelation values in the spatial domain to find potential regularities. We just need the maximum spectral density value. Frequency analysis allows a more efficient way to perform peak finding and translation symmetry detection from the frieze-expansion.

3.3. Rotation Symmetry Strength (RSS) Map

If there is only one dominant coefficient in the DFT space, we can conclude that there is a symmetry. This is usually the case with synthetic images like Figure 1. Natural images usually show multiple dominant coefficients. We calculate rotation symmetry strength (RSS) from the DFT coefficients. RSS is a function of center position, radius r and angular step size θ. In the rotation center detection step of our algorithm, the maximum radius inside the given image for each location is used and the angular step size is fixed to $2\pi/N$. By fixing these parameters, RSS becomes a function of position only and can be represented as a two dimensional intensity map or RSS map. The 1st DC coefficient is not used for RSS calculation.

Let $S_{x,y,r}(k)$ represent the kth spectral density of the rth row of the frieze pattern at the center (x,y). With the angular step size $2\pi/N$, we have N points for each row of the frieze pattern and also N coefficients for each corresponding row of the DFT result (Figure 3(b), (c)).

$$\{S_{x,y,r}(1), S_{x,y,r}(2), \cdots, S_{x,y,r}(N)\} \quad (4)$$

First, the dominant density $S_{x,y,r}^d$ among the first half of the energy spectrum satisfy the following condition:

$$S_{x,y,r}^d(i) > mean(S_{x,y,r}(k)) + \alpha \cdot std(S_{x,y,r}(k)) \quad (5)$$
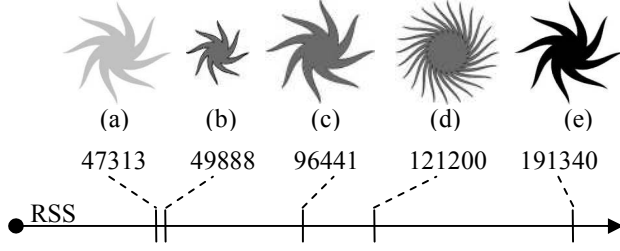$$k = 2,3,4,\cdots,N/2$$

Figure 6: RSS value is a function of size ((b) vs (c)), # of fold ((c) vs (d)) and intensity contrast ((a) vs (c) vs (e)).

The existence of these dominant coefficients, however, does not always indicate the existence of a symmetry. We need to check the coincidence of k dominant coefficients to confirm that all indices of dominant coefficients are multiples of the smallest index. If all indices of dominant peaks satisfy this condition, we conclude that there is a rotational symmetry in the row. The RSS measure at position (x, y) is defined as,

$$RSS(x,y) = \sum_{r=1}^{R} \rho_r \frac{mean(S_{x,y,r}^d(j))}{mean(S_{x,y,r}^{others}(i))} \qquad (6)$$

$$\rho_r = \begin{cases} 1 & \text{, if } Modulus(S_{x,y,r}^d, \min(S_{x,y,r}^d)) = 0 \\ 0 & \text{, otherwise} \end{cases}$$

where R is the total number of row of the frieze pattern. By computing the RSS score for expanded frieze patterns around the candidate rotation centers throughout the whole image, we can build a dense rotational symmetry strength map for the given image. This RSS map provides a quantitative symmetry measure at each pixel. Figure 3(d) shows an example of the RSS map overlaid on the original image, Figure 3(a). Higher values of RSS mean stronger likelihood of rotation symmetry at that location. Figure 6 shows that higher fold, higher contrast and bigger region sizes contribute to higher RSS values, signifying a perceptually more symmetric pattern.

3.4. Hierarchical Search

Even though a full search at each pixel gives a more accurate RSS map, the processing time increases linearly with the image size. We use a hierarchical search algorithm to accelerate the rotation symmetry center detection process.

We start from the observation that most rotation symmetry remains when an image is scaled down. Gradually reducing the size of the original input image, we form an image pyramid. We perform full search over the smallest image at the top of the pyramid. The initial RSS map provides several local peaks forming the potential centers of rotation symmetries. The initial symmetry map is
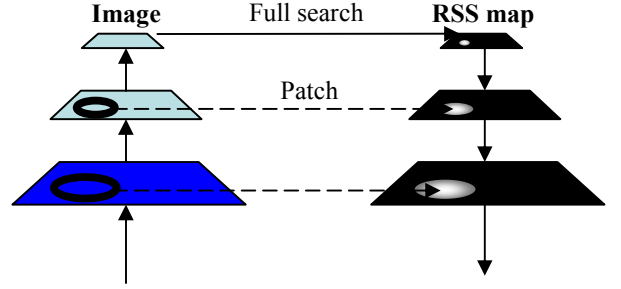

Figure 7: A hierarchical search is used to efficiently detect candidate symmetry centers at the highest resolution.

then enlarged using bilinear interpolation to the size of the next level of the pyramid. Previously detected center candidate points and their neighborhood regions are then refined with image patches at a higher resolution level. This process is repeated until we reach the original image resolution (Figure 7). After we reach the final, highest resolution RSS map, we select the final candidate symmetry center points.

The RSS map can be thought of as a symmetry saliency map, and we adopt a well-known peak visiting method called the inhibition-of-return mechanism [8] to extract local maxima in descending order of saliency. We continue to extract local maxima until the RSS value falls below a threshold, $mean(RSS) + \beta \cdot std(RSS)$ [15]. Ideally, the optimal values of α (equation 5) and β can be determined by the RSS range within which the human eye can perceive a rotation symmetry. In our experiments, we use empirical values of 2 and 1.8 for α and β respectively for all images.

4. Symmetry Group Analysis

After rotation symmetry center detection, the DFT spectral density of each frieze-expansion is used to determine the number of fold, symmetry group types and the symmetry support region. The DFT spectral density image (Figure 3(c)) contains frequency information of each row, corresponding to each concentric band in the original image. This makes it possible to analyze in detail the symmetry of image patches around a given center.

4.1. DFT Segmentation

As can be seen in Figure 3(c), several consecutive rows may have the same peak distributions of DFT spectral density. This indicates a "frequency cluster" leading to one contiguous symmetry-supporting region. We can therefore differentiate one symmetry region from another type of symmetry region (bands) even though they share the same center. By grouping consecutive dominant peaks, we can delineate each symmetry region on both the converted frieze

pattern and the original image. Figure 3(c) shows a segmented result. Figure 3(e) shows the summed DFT power spectrum of corresponding symmetry regions, from which we can decide the number of fold, as described next.

4.2. Number of Folds

From the DFT coefficient plot of each supporting region, we find the highest coefficient basis k. The number of fold corresponds to k-1. Note that we only consider AC coefficients. For example, the 7th bases are cosine/sine waves with six cycles. This responds most strongly to six-fold rotation symmetry. In Figure 3, the summed up DFT density plot in (e) has a maximum peak at the 6th component and (g) has its maximum peak at the 5th component, which represents a 5-fold and a 4-fold rotation symmetry, respectively. The reader can verify this with respect to the corresponding frieze patterns in Figure 3(h) and (j). Figure 8 shows several fold decision examples from the DFT spectral density image.

We can prove that if a frieze expansion has horizontal reflection symmetry along the center row (Figure 3(b)), the inverse frieze expansion in its image space has a rotation symmetry with even fold, otherwise it is odd. For example, the pattern in Figure 3(j) is reflected symmetrically in figure 3(b), but the pattern in 3(h) is not. This helps to decide robustly the number of fold.

4.3. Symmetry Group Classification

From the observation of Figure 3(h) and (j), we know that a frieze-expansion pattern of cyclic symmetry has no vertical reflection, while a frieze-expansion pattern of dihedral symmetry have to have vertical reflection. By checking the existence of vertical reflection in a frieze pattern, we can differentiate cyclic from dihedral symmetry. Furthermore with the fold information, we can identify the motif of a frieze pattern [9] computationally. By flipping a
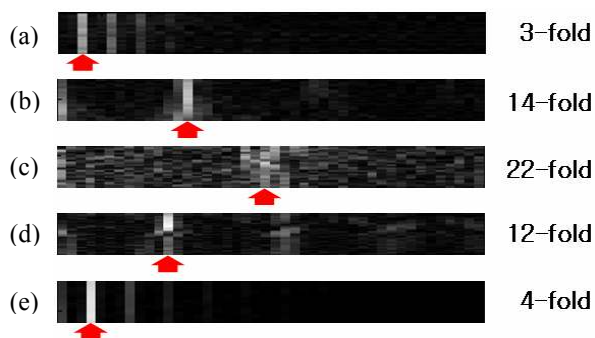

Figure 8: Number of fold decision from DFT result. All DFT results are from our test images I-1, I-11, I-12, I-2 and I-5, respectively (Figure 9). Red arrows indicate the dominant coefficient, each of which corresponds to (a) 4th, (b) 15th, (c) 23th, (d) 13th and (f) 5th DFT coefficient.

Method	GVF[1]	SIFT[3]	Ours
Center	44 %	85 %	82 %
Fold	N/A	39 %	84 %
Cyclic/ Dihedral	N/A	N/A	88 %

Table 2: Quantitative experimental comparison on 80 images. Success rate is based on the true positive detection result.

motif horizontally and sliding it over the frieze pattern while calculating correlation, we can verify whether there is a periodic match or not. If there is, we conclude this region is dihedral, and if not, cyclic. In other words, if there is vertical reflection in the frieze pattern, it falls into the dihedral rotation symmetry group.

One exceptional case is shown in Figure 3(f). Most of the coefficients are zero, signifying that the corresponding region of the original image is uniform, as in Figure 3(i). This indicates the existence of the continuous rotation symmetry group, O(2).

4.4. Merging and Elimination

Our algorithm investigates symmetry for each row in the expanded frieze pattern. Noise can cause detection failure in a narrow band and this could divide one symmetry region into multiple regions, even though they have the same symmetry characteristics. To avoid this, we merge consecutive symmetry regions if they share the same number of fold and symmetry type.

For the same reason, a narrow region could be selected as one symmetry region even though it is not a symmetric region or is a symmetry region that is hardly perceived by the human eye due to its narrow width. We eliminate such narrow symmetry regions in post-processing.

5. Experimental Result

We tested our algorithm on 80 images of various types to verify the strength and weakness of our algorithm. Figure 9 shows 18 sample results. Each image presents some type of computational challenge in symmetry detection, such as intensity/color variation (I-1, I-4), concentric symmetry (I-3, I-6), minimum texture (I-5), continuous symmetry (I-7), occlusion (I-12, I-17), high order of symmetry (I-12, I-13), multiple symmetry types (I-3, I-6, I-14) and no symmetry (I-18). Our algorithm detects the rotation symmetry correctly under these adverse conditions. Test image I-5 contains no texture, but our algorithm can perceive 4-fold rotation symmetry by its shading gradation. Test image I-12 and I-17 show that our algorithm is robust to occlusion. This is because the non-occluded parts still maintain regularity and respond strongly to the corresponding cosine/sine waves in the DFT bases. Test image I-18 has no rotation

symmetry in it, and our algorithm gives a null result.

Table 2 shows quantitative comparison results of our proposed algorithm and two state of the art rotational symmetry detection algorithms [1, 3].

One limitation of our algorithm is that it fails to find a correct center of rotation when the symmetry object is skewed so that the frieze-expansion of the object shows distorted translation symmetry. In I-14, one small cactus at the left upper corner is out of the search range and two other small cacti are not detected. Skewing of the texture (inside of I-11 and I-17) causes a wrong fold detection result. One starfish of I-16 has a D6 result because one leg of another starfish is nearby, so the starfish looks like it has 6 legs.

6. Conclusion

We introduce a novel and effective rotational symmetry detection algorithm. Frieze expansion and its analysis reveal the close relation between rotation symmetry groups and frieze groups. Guided by this tight coupling of two distinct types of symmetry groups and using the discrete Fourier transform (DFT), we build a rotation symmetry strength (RSS) map over the whole image. Our algorithm converts all spatial domain information into the frequency domain using DFT, which decomposes the frieze-expansion of the original image into a mixture of sine and cosine waves representing different types of symmetries in the original image. Our method has a time complexity independent of the rotation symmetry fold number and image complexity (Table 1). Our algorithm is simple to implement and detects centers of rotation symmetries, rotation group types, concentric symmetries and order of symmetry groups. Experimental results on a dataset of synthetic and natural images show the superiority of our algorithm over previous state-of-the-art algorithms (Table 2). All test images and more experimental results can be found at our research webpage (http://vision.cse.psu.edu/rotsym.htm).

Acknowledgement

References

[1] Gareth Loy and Jan-Olof Eklundh, Detecting Symmetry and Symmetric Constellations of Features, Proceedings of ECCV, 2006, pp. 508-521.

[2] Hugo Cornelius and Gareth Loy, Detecting Rotational Symmetry Under Affine Projection, 18th International Conference on Pattern Recognition (ICPR '06) pp. 292-295.

[3] V. Shiv Naga Prasad and Larry S. Davis, Detecting Rotational Symmetries, ICCV, 2005, pp. 954-961

[4] Y. Liu, J.H. Hays, Y. Xu, and H. Shum, Digital Papercutting, Technical Sketch, SIGGRAPH 2005.

[5] Y. Keller and Y. Shkolnisky. A signal processing approach to symmetry detection. IEEE Transactions on Image Processing, 15(8):2198–2207, 2006.

[6] L. Itti, C. Koch, and E. Niebur, A Model of Saliency-Based Visual Attention for Rapid Scene Analysis, IEEE Transactions on Pattern Analysis and Machine Intelligence, Vol. 20, No. 11, Nov 1998

[7] Y. Liu, R. Collins, and Y. Tsin, "A Computational Model for Periodic Patern Perception Based on Frieze and Wallpaper Groups", IEEE Transactions on Pattern Analysis and Machine Intelligence, Vol. 26, No. 3, March, 2004, pp. 354 – 371

[8] I. Hargittai and M. Hargittai, Symmetry: A Unifying Concept, Bolinas, California: Shelter Publications, 1994.

[9] C. Sun and J. Sherrah, 3D Symmetry Detection Using The Extended Gaussian Image, IEEE Transactions on Pattern Analysis and Machine Intelligence, Vol. 19, No. 2, Feb, 1997, pp. 164 – 168

[10] G. Marola. On the detection of the axes of symmetry of symmetric and almost symmetric planar images. IEEE Transactions on Pattern Analysis and Machine Intelligence, 11(1):104–108, January 1989.

[11] Stéphane Derrode, Faouzi Ghorbel, Shape analysis and symmetry detection in gray-level objects using the analytical Fourier-Mellin representation. Signal Processing 84(1) 25-39 (2004).

[12] Rafael C. Gonzalez, Richard E. Woods, Digital Image Processing. 2nd Edition, 2002, ISBN 0-20-118075-8.

[13] John G. Proakis and Dimitris G. Manolakis, Digital Signal Processing. Principles, Algorithms, and Applications. Third Edition. 1996, ISBN 0-13-373762-4.

[14] H. Weyl. Symmetry. Princeton University Press, Princeton, New Jersey, 1952.

[15] Z. Zhang, Parameter Estimation Techniques: A Tutorial with Application on Conic Fitting, Image Vis. Computing, vol. 15, pp. 59–76, 1997.

[16] Locher, P., Nodine, C, Symmetry catches the eye. Eye Movements: from Physiology to Cognition, O'Regan, J. and Levy-Schoen, A., Elsevier Science Publishers B.V. ,1987

[17] M. Park, S. Lee, P. Chen, S. Kashyap, A. Butt and Y. Liu, Performance Evaluation of State-of-the-Art Discrete Symmetry Detection Algorithms, Proceedings of IEEE CVPR 2008, Anchorage, Alaska, USA, June 2008

Synthetic image				Natural image			
Desc.	Image	RSS map	Result	Desc.	Image	RSS map	Result
[I-1] C3				**[I-10]** D4 No symmetry inside			
[I-2] D12				**[I-11]** C14			
[I-3] D4,C5 SO(2) Concentric symmetries				**[I-12]** D22 Occlusion High texture			
[I-4] C3 Different color				**[I-13]** D33 High fold High texture			
[I-5] D4 No texture				**[I-14]** D12,D13 Multiple skewed			
[I-6] C3,C6 C4,C5 Concentric symmetries				**[I-15]** D13 skewed			
[I-7] SO(2) No texture				**[I-16]** D5 Multiple centers			
[I-8] D4,D8 Wall paper (P4M) Multiple centers				**[I-17]** D High texture Occlusion			
[I-9] C6,C3 Wall paper (P6) Multiple centers				**[I-18]** Random noise (No Symmetry)			

Figure 9: Experimental results on 16 sample images. Each image demonstrates different types of symmetry characteristic and challenging conditions. Most detection results show correct center location and symmetry regions, regardless of image and symmetry type. See text for more discussion of these results.